Fluorescent imaging of heavy charged particle tracks with LiF single crystals

Paweł Bilski[a,*], Barbara Marczewska[a], Wojciech Gieszczyk[a], Mariusz Kłosowski[a], Michał Naruszewicz[a], Małgorzata Sankowska[a], Satoshi Kodaira[b]

[a] Institute of Nuclear Physics, Polish Academy of Sciences (IFJ PAN), 31-342, Kraków, Poland
[b] National Institute of Radiological Sciences (NIRS) / QST, Chiba, Japan

ARTICLE INFO

ABSTRACT

Radiophotoluminescence of F_2 and F_3^+ color centers in LiF was exploited for imaging tracks of energetic heavy charged particles. LiF crystals were irradiated with helium, carbon, neon, silicon and iron ions at the HIMAC accelerator in Chiba, Japan. The patterns created by radiation were visualized with a wide-field fluorescent microscope under blue-light excitation. The shape of the visible tracks was found not to depend on ion type and energy. The full width at half maximum of track profiles was in all cases around 500 nm, what corresponds with the resolution limit of the microscope, which was estimated to be 420 nm. On the other hand the fluorescent intensity of tracks was found to increase in a linear manner with the increasing LET. This indicates possibility of obtaining some spectrometric information on the radiation field.

1. Introduction

Fluorescent imaging of the tracks produced by charged nuclear particles is an original method developed by Akselrod and co-workers using C and Mg-doped aluminium oxide crystals [1–4]. The crystals used for this purpose have been called Fluorescent Nuclear Track Detectors (FNTD) and under this name the technique became widely known. The idea of the method is based on fluorescence (photoluminescence) of color centers created by ionizing particles on their path through a crystal. A single heavy charged particle deposits only a small amount of energy in an also small volume (typically between 1 keV/μm and 1 MeV/μm in a track of diameter usually well below 100 nm). As a consequence the number of the created optically active color centers must be also small. Photoluminescence yield of color centers in Al_2O_3 and sensitivity of the modern fluorescent microscopes were however found to be sufficiently high to detect and image weak fluorescent patterns produced by these particles. In some cases even electron tracks could be observed.

For over a decade since the development of FNTDs, Al_2O_3 single crystals remained the only material which could be used for this purpose. This situation has changed only recently, when lithium fluoride crystals were successfully applied as FNTDs [5–8]. Radiophotoluminescence of color centers in LiF is a well-known and studied already for decades phenomenon [9–12]. Ionizing particles penetrating LiF crystals produce lattice defects, which mainly consists of F centers (electron trapped by an anion vacancy) and H centers (interstitial

fluorine atom). These defects in turn tend to form more complex aggregates. A typical absorption spectrum of an irradiated LiF crystal exhibit two main bands at about 250 nm (attributed to F center) and at 445 nm (attributed to so called M center, which in fact represents F_2 and F_3^+ defects). Less intense, but also often visible, are bands at 317 nm and 377 nm (attributed to F_3, sometimes called R center). All these defects are thermally stable up to temperature of about 400 K and for higher temperatures their gradual decomposition occurs [13]. While F center does not produce any photoluminescence, the excitation of M centers with the blue light leads to strong photoluminescent emission within two bands: green (peaked near 520 nm, corresponding to F_3^+) and red (peaked near 670 nm, corresponding to F_2). This photoluminescence of LiF was exploited for obtaining images of nuclear particles tracks.

The performed so far investigations of LiF crystals as FNTDs were focused mainly on imaging low-energy radiation emitted by radioisotope sources: alpha particles and neutrons (the latter through secondary particles, the products of nuclear reactions with ^{6}Li nuclei). The goal of the present work are analyses of the fluorescent patterns produced in LiF by various high energy ions (fully ionized nuclei).

2. Materials and methods

LiF single crystals were grown at the IFJ PAN with the Czochralski method in argon atmosphere, using undoped LiF powder as a starting material. The samples used in measurements consisted of transparent

Fig. 1. LiF crystal samples: a) samples after polishing, b) a sample illuminated through the objective of the Nikon Eclipse Ni–U fluorescent microscope, c) a close-up of the illuminated sample.

square plates (typical size about $4 \times 4 \times 1$ mm), which were cut with diamond saws from the as-grown crystals and then polished with fine abrasive strips (Fig. 1a). Prior to further investigations, the crystal samples were pre-heated at the temperature close to LiF melting point (820–830 °C) for 10 min. This treatment improved quality of the crystal surface by removing small scratches left by polishing.

Irradiations of LiF crystal samples with high-energy ions were conducted at the Heavy Ion Medical Accelerator (HIMAC) in Chiba, Japan, within three experimental sessions over years 2017–2018. The following ion species were exploited: helium, carbon, neon, silicon and iron. The details of the used ion beams are given in Table 1. The values of the linear energy transfer (LET) and particle ranges given in Table 1 and all others used within this work were calculated with the SRIM code [14]. Besides irradiations with the pristine ion beams, some of the exposures were performed using PMMA absorbers, degrading ions energy. Fig. 2 presents depth-dose distributions (Bragg curves) for the exploited ion beams, as well as it indicates positions along these curves (i.e. thickness of the used absorbers) at which the samples were placed for irradiations. The irradiations were done with the particle fluence at the level of $10^5 \, \text{cm}^{-2}$. During the exposures, a part of the crystal samples was positioned perpendicularly, while another part parallel to the ion beam direction. The geometrical arrangement is illustrated in Fig. 3, together with examples of the obtained track images. Besides irradiations with energetic ions, some complementary exposures were performed with alpha particles from ^{241}Am source.

Microscopic fluorescent images of LiF crystals were acquired using a Nikon Eclipse Ni–U upright fluorescence wide-field microscope with a DS-Qi2 CCD camera (see Fig. 1b and c). For excitation the pE-100

Table 1

Parameters of the used ion beams at HIMAC accelerator. Nominal energy concerns ions at the accelerator output, while actual energy, ions at the experimental positions (accounts for energy losses in air, beamline window, etc. and in the PMMA absorber layer, if used). Values of LET in water are also given, as this quantity is commonly used to characterize a beam in dosimetric and medical applications. LET and range values refer to the actual energy of particles.

| Ion	Nominal energy MeV/n	Absorber layer mm	Actual energy MeV/n	LET LiF keV/μm	LET H_2O keV/μm	Range in LiF mm
^{4}He	150	–	143.8	4.8	2.26	68.6
		100.42	74.1	7.8	3.69	21.2
^{12}C	290	–	274.2	27.8	13.1	70.7
		100.42	144.0	42.1	19.9	23.4
		147.29	27.9	148.0	70.8	1.26
^{20}Ne	400	–	367.5	66.8	31.4	67.9
		130.44	93.5	162.5	76.8	6.5
^{28}Si	490	–	441.3	121.3	57.0	64.3
^{56}Fe	500	–	412.5	423.3	199	34.3
		59.64	148.6	775	366	6.3
		60.32	144.6	788.7	372	6.0
		69.59	66.1	1394	660	1.58
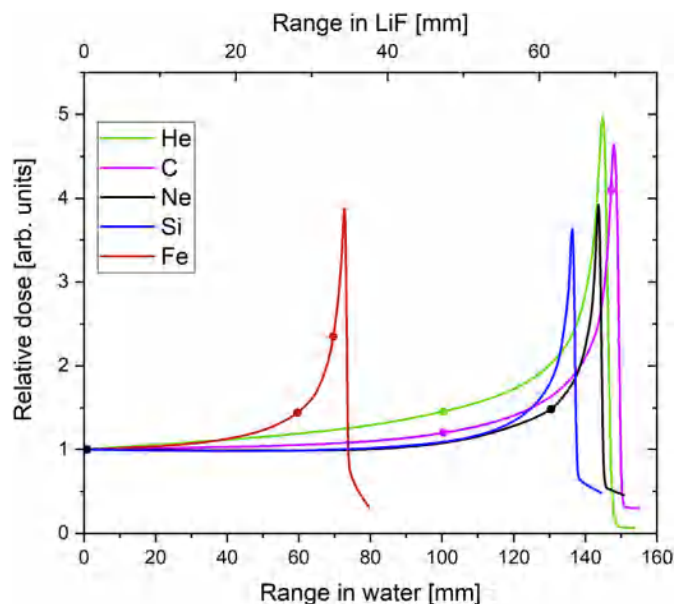
Fig. 2. Depth-dose distributions in water for the used ion beams (measured with an ionization chamber), normalized to the entrance dose (at zero depth). The solid circles indicate thickness of the absorbers applied for irradiations of the samples. The top axis illustrates equivalent ion ranges in LiF.

illumination system with 440 nm LEDs (CoolLED) was used. A band-pass filter ET445/30 was used for excitation light, while long-pass ET570lp for emission. The observations were conducted with 100 × TU Plan ELWD (NA 0.80) objective lens. The acquisition time varied between 5 s and 40 s depending on the brightness of the observed tracks, but intensity of images was then normalized to unit time. Image analysis were realized with the Nikon NIS-Elements and with the Fiji software [15]. The photoluminescence emission spectra were measured using Ocean Optics QE pro 00689 spectrometer.

3. Results and discussion

The shape of the photoluminescence emission spectrum of LiF (proportion between F_2 and F_3^+ bands) is known to depend on illumination wavelength and intensity [16,17]. It was therefore important to perform spectral measurements in conditions possibly similar to those used for FNTD imaging. For that reason, the spectrometer was mounted onto the microscope in place of the CCD camera and in this way exactly the same light source, lenses, filters and dichroic mirror were applied. However, doses (particle fluence) achieved with energetic ions at HIMAC, were too low to enable spectrum measurements. Instead of energetic ions, alpha particles from ^{241}Am source were therefore used. Fig. 4 presents photoluminescence emission spectrum of LiF following irradiation with alpha particles. It is apparent that in the
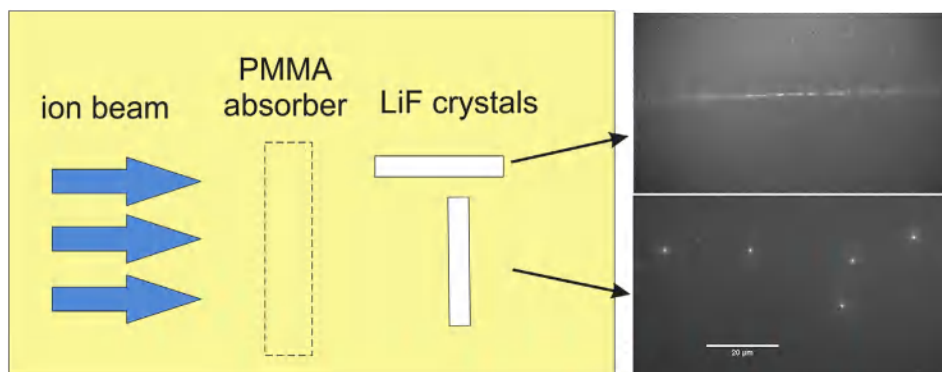
Fig. 3. Illustration of the geometrical arrangement of the samples during ion beam irradiations. On the right side examples of the track images of Ne ions obtained for two positions of crystals with respect to the beam direction: nearly parallel (top) and perpendicular (bottom).
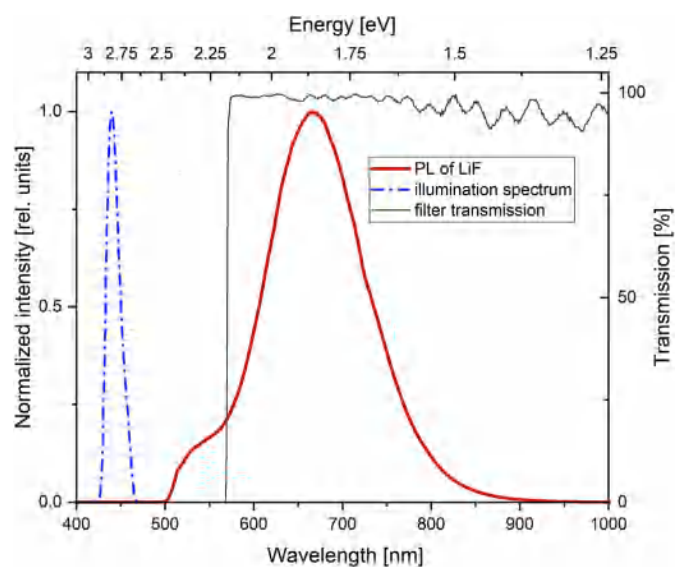
Fig. 4. Normalized PL emission spectrum of the alpha irradiated LiF crystal The applied spectrum of the excitation light is also presented, as well as the transmission curve of the long-pass filter ET570lp, which was used in further measurements (according to the producer data: www.chroma.com).

applied experimental conditions F_3^+ band around 520 nm is quite weak and its input to the total signal is small. It was therefore decided to use a long pass filter with the edge set at a higher wavelength (ET570lp), so cutting off the F_3^+ band, but achieving better discrimination from the illumination light. The correctness of this approach was then confirmed during observations with the CCD camera, as acquired images exhibited lower background and better contrast, than when filters with the edge closer to 500 nm were used.

Fig. 5 shows examples of images of tracks produced by various ion beams directed perpendicularly to the crystal surface. These particular images were processed with the Background Subtractor plugin to the Fiji software [18]. This procedure allows to obtain good quality images, however it is time consuming and was found to introduce sometimes significant deformations to the original images, therefore it was not applied in quantitative analysis. All images presented in Fig. 5 were registered at identical experimental conditions and were all processed in the same way, therefore the apparent differences between the tracks reflect real physical effects. The tracks produced by particles with higher LET seem to be larger, but this is a somewhat misleading impression. The actual size of all tracks is basically identical, the difference is only in fluorescent intensity. This is well illustrated in Figs. 6 and 7. The data plotted in these figures were obtained by averaging for each track the profiles measured along diameter lines drawn at sixteen

different angles through a track center. Fig. 6 presents raw data, i.e. without subtracting background. In this way the ratios between maximum track intensities and background levels are also demonstrated. For the He tracks, which exhibited the weakest fluorescence, this intensity exceeds background by only 10–20%. Fig. 7 presents for a few selected ion species the same data after subtracting the background baselines, showing that the shape of the tracks is indeed identical. The shape of the peaks formed by a track profile does not follow the typical gaussian function: it is very narrow near maximum, but with long tails at larger distances from the center. These peaks may be quite well described by the Pearson VII distribution function, as illustrated in Fig. 8. The full width at half maximum (FWHM) of the peaks is equal to about 500 nm. This value corresponds well with the resolution of the microscope. Estimating the resolution as λ/2NA, for the applied objective (NA = 0.80) and λ = 670 nm one gets 419 nm. The lack of differentiation of shape and size between tracks of various ions is actually an expected effect. The real size of a track produced by a heavy charged particle is much smaller than the resolution limit of the microscope. This size may be estimated for example by radius around a particle path in which 90% of the dose is deposited. Performing such calculations with the Libamtrack code [19], in which various models of radial dose distribution are implemented, produces values ranging from single nanometers up to about 30 nm, depending on the applied model and its parameters. For the used microscope such nuclear particles tracks are therefore basically point sources of light and broadening of their images is due to optical effects: diffraction and possibly light scattering. The latter effect is probably the reason of quite long tails observed in the track profiles, which extend for several micrometers. Similar analysis of track size were performed by Niklas et al. [20] for aluminium oxide FNTDs. For a confocal microscope, with resolution estimated as 320 nm, they observed a negligible dependence of track size on LET, similarly as in the present work. For the superresolution STED microscopy, which resolution power was found to be 80 nm, such dependence was apparently present.

The dependence of track intensity on ionization density may be quantified by plotting maxima of track profiles versus LET (Fig. 9). For the intermediate LET values (ranging between C and Fe primary beams) the data points follow perfectly the linear trend. The fitted function possesses a non-zero intercept parameter b, what may suggest, that the applied method of subtracting background as a baseline of the track profile, is not fully effective. For the highest LET values (Fe beam after crossing 50–70 mm of water equivalent) the data points lie below the trend line. This might be caused by the saturation of photoluminescence in the core of tracks due to extremely high doses. On the other hand one has to remember that these data points might be biased by larger uncertainties, as the exposures were done near the Bragg peak, therefore in conditions of very steep changes of energy and ionization density. This issue requires further investigations. For the lowest LET values (below 10 keV/μm) the detection limit seems to be achieved. Both data

Carbon: 27.8 keV/μm   Carbon: 42.1 keV/μm

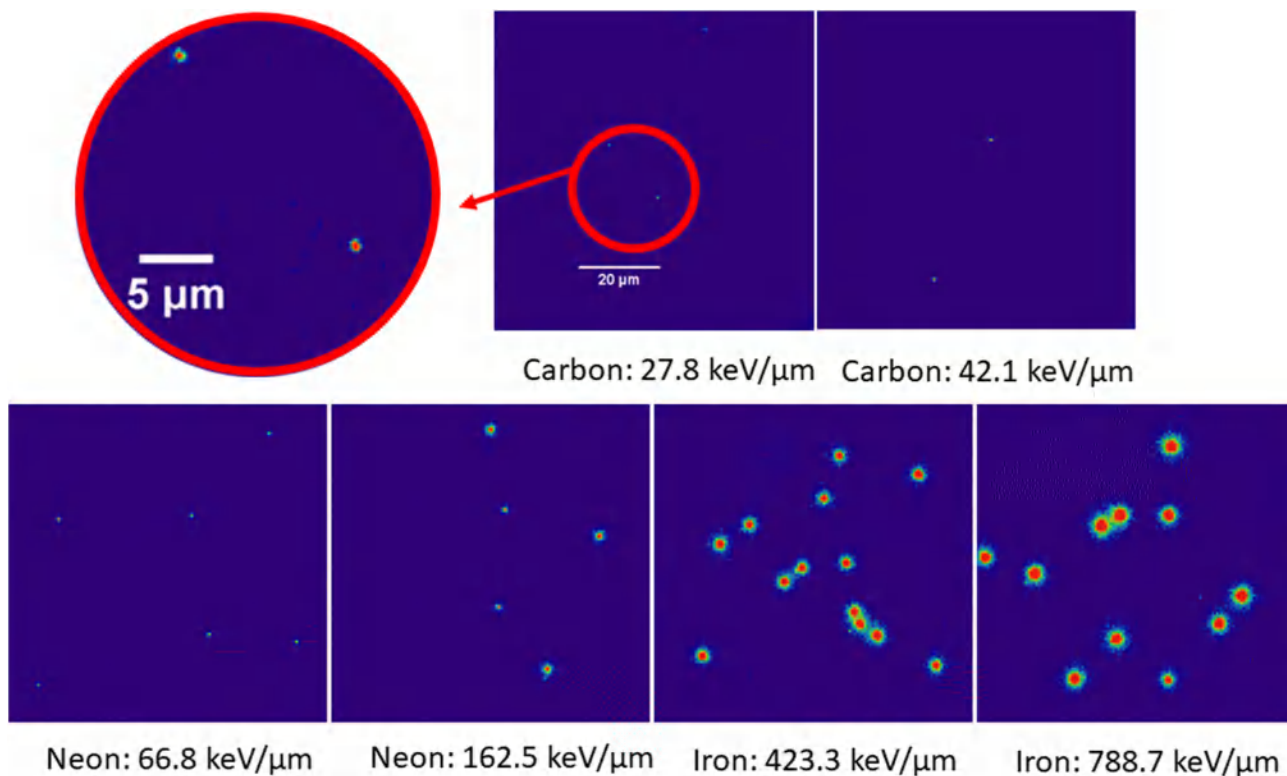Neon: 66.8 keV/μm   Neon: 162.5 keV/μm   Iron: 423.3 keV/μm   Iron: 788.7 keV/μm

Fig. 5. Examples of track images for ion beams directed perpendicularly to the crystal surface. The given values of ionization density represent LET in LiF.
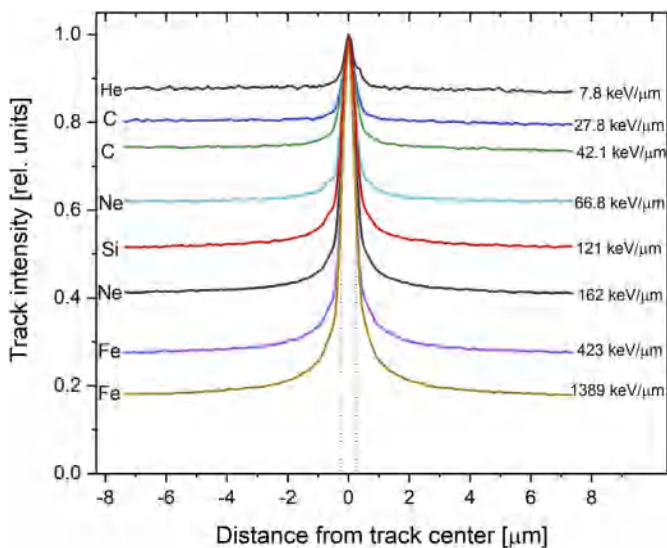

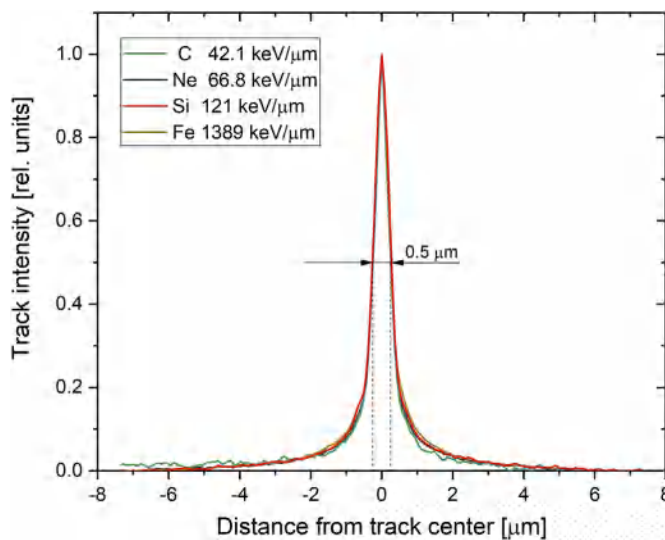**Fig. 6.** Radial profiles of tracks (intensity normalized to maximum).

Fig. 7. Radial profiles of the selected tracks after subtracting background baselines (intensity normalized to maximum). FWHM of the peaks is equal to about 0.5 μm.

points obtained for He ions show the same track intensity, which, as was mentioned before, exceeds background level by only 10–20%. The improvement of the detection limit would require increasing of the signal to noise ratio.

The discussed so far tracks originated from the samples irradiated with the ion beams directed perpendicularly to the crystal surface and consequently the tracks had shape of circular spots. In case of the samples positioned approximately parallel to the ion beam, the produced tracks have shape of lines. As positioning of the samples was usually not ideally parallel, but rather under a small angle to the beam, and because of the very short focal depth of the microscope (below 1 μm), typically only part of a track is in focus. This effect can be observed for example in the upper image of Fig. 3 and it is presented in a

more apparent way in Fig. 10a for iron ions. A sharp image of the track produced by a particle which crossed the crystal under an angle, may be obtained if not a single image, but a stack of images is acquired, taken with small vertical steps. Such a 3D dataset may be then projected on a 2D plane using so called maximum intensity projection. The pixels belonging to the parts of an image which are in focus are brighter than those being out of focus, therefore such operation reconstructs a sharp image of a whole track. In this way the image presented in Fig. 10b was obtained. It shows tracks of two carbon ions. One of them (upper) stops within the field of view, while the second, having somewhat higher energy, travels further. Fig. 10c presents tracks of two neon ions. The particularly remarkable is the visible track of a delta electron. Several
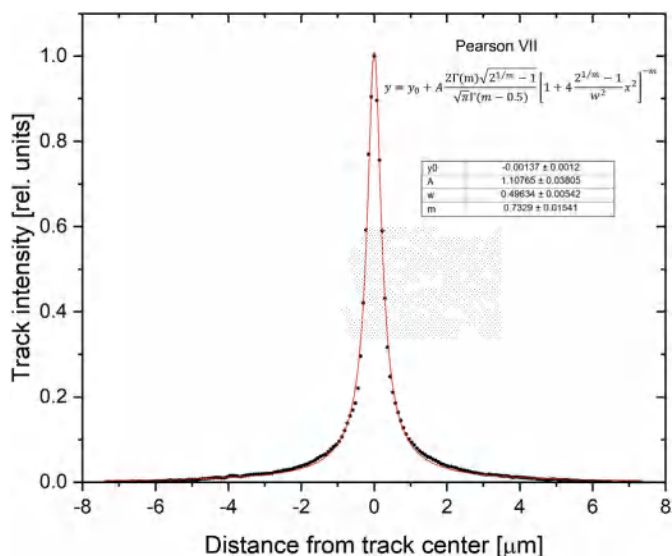
Fig. 8. Radial profile of a Fe track (1389 keV/μm) fitted with the Pearson VII distribution function.
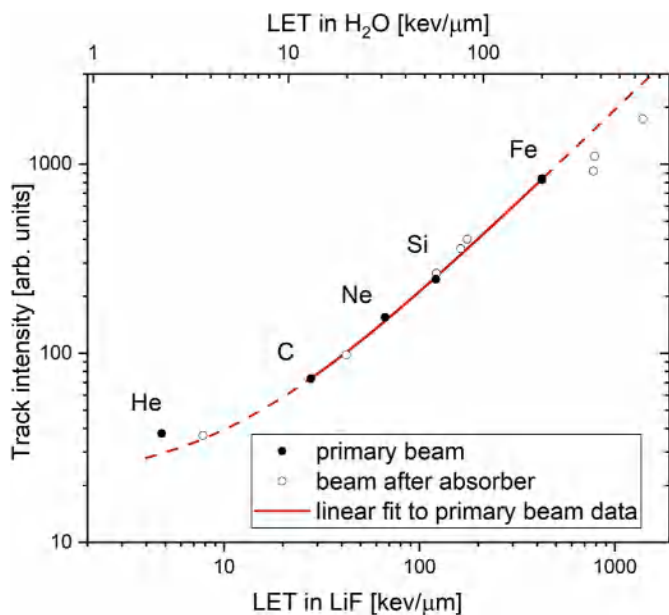

Fig. 9. Track intensity vs. LET in LiF. The line represents a linear fit to the primary beam data points (without He), with parameters $a = 1.92$, $b = 20.25$. Uncertainty bars not plotted for clarity.

other bright spots are also noticeable, which seem to be related to secondary particles as well. All tracks show strong fluctuations of photoluminescence intensity with their length (the same pertains also for not shown tracks of other ions). The reasons of these fluctuations are not yet clear – several effects may be considered, like irregularities of energy deposition, nonuniformity of a crystal properties, optical effects.

4. Conclusions

The performed investigations confirmed usefulness of lithium fluoride FNTDs for detection of energetic heavy charged particles. The tracks of all tested particles, which were ranging from helium to iron nuclei, were successfully visualized. Particles with LET at the level of several keV/μm, like energetic helium ions, seem to represent the currently achievable lower detection limit of the technique. The improvement in this aspect would require increasing of the signal to noise
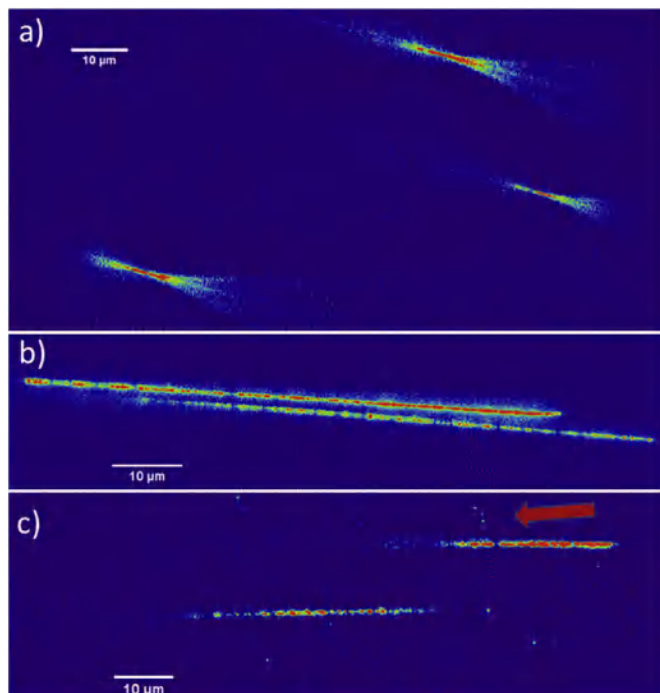

Fig. 10. Examples of nearly parallel tracks: a) iron ions (energy at entering crystal 145 MeV/nucleon), b) carbon ions stopping within LiF crystal (maximum intensity projection of 10 images taken with 1 μm steps), c) neon ions (energy at entering crystal 93.5 MeV/nucleon); the arrow indicates a delta electron track. Color scale arbitrary and different for each image. Background was numerically subtracted.

ratio. The observed size of the fluorescent tracks does not depend on the particle energy nor LET. This is explained by the optical resolution limit (c.a. 400 nm), which is much larger than the diameter of the original tracks produced by the studied nuclear particles in LiF crystals. On the other hand fluorescent intensity of tracks increases in a linear manner with the increasing LET. This suggests possibility of extracting some spectrometric information on the radiation field, what however requires further work on development of appropriate methods of analysis.

References

[1] G.M. Akselrod, M.S. Akselrod, E.R. Benton, N. Yasuda, A novel Al_2O_3 fluorescent nuclear track detector for heavy charged particles and neutrons, Nucl. Instrum. Methods B 247 (2006) 295–306.

[2] M. Akselrod, J. Kouwenberg, Fluorescent nuclear track detectors – review of past, present and future of the technology, Radiat. Meas. 117 (2018) 35–51.

[3] M.S. Akselrod, A.E. Akselrod, New Al_2O_3:C,Mg crystals for radiophotoluminescent dosimetry and optical imaging, Radiat. Protect. Dosim. 119 (2006) 218–221.

[4] A. Neuholz, S. Greilich, Assessment of microscopic ion beam field variation using fluorescent nuclear track detectors, Radiat. Meas. 106 (2017) 595–601.

[5] P. Bilski, B. Marczewska, W. Gieszczyk, M. Kłosowski, T. Nowak, M. Naruszewicz, Lithium fluoride crystals as fluorescent nuclear track detectors, Radiat. Protect. Dosim. 178 (2018) 337–340.

[6] P. Bilski, B. Marczewska, M. Kłosowski, W. Gieszczyk, M. Naruszewicz, Detection of neutrons with LiF fluorescent nuclear track detectors, Radiat. Meas. 116 (2018) 35–39.

[7] P. Bilski, B. Marczewska, Fluorescent detection of single tracks of alpha particles using lithium fluoride crystals, Nucl. Instrum. Methods B 392 (2017) 41–45.

[8] P. Bilski, B. Marczewska, W. Gieszczyk, M. Kłosowski, M. Naruszewicz, Y. Zhydachevskyy, S. Kodaira, Luminescent properties of LiF crystals for fluorescent imaging of nuclear particles tracks, Opt. Mater. 90 (2019) 1–6.

[9] J. Nahum, D.A. Wiegand, Optical properties of some F-aggregate centers in LiF, Phys. Rev. 154 (1967) 817–830.

[10] G. Baldacchini, Colored LiF: an optical material for all seasons, J. Lumin. 100

(2002) 333–343.

[11] R.M. Montereali, S. Almaviva, F. Bonfigli, A. Cricenti, A. Faenov, F. Flora, P. Gaudio, A. Lai, S. Martellucci, E. Nichelatti, T. Pikuz, L. Reale, M. Richetta, M.A. Vincenti, Lithium fluoride thin-film detectors for soft X-ray imaging at high spatial resolution, Nucl. Instr. Meth. A 623 (2010) 758–762.

[12] R.M. Montereali, A. Ampollini, L. Picardi, C. Ronsivalle, F. Bonfigli, S. Libera, E. Nichelatti, M. Piccinini, M.A. Vincenti, Visible photoluminescence of aggregate colour centres in lithium fluoride thin films for low-energy proton beam radiation detectors at high doses, J. Lumin. 200 (2018) 30–34.

[13] K. Schwartz, A.E. Volkov, M.V. Sorokin, R. Neumann, C. Trautmann, Effect of irradiation parameters on defect aggregation during thermal annealing of LiF irradiated with swift ions and electrons, Phys. Rev. B 82 (2010) 144116.

[14] J.F. Ziegler, M.D. Ziegler, J.P. Biersack, SRIM - the stopping and range of ions in matter, Nucl. Instrum. Methods B 268 (2010) 1818–1823.

[15] J. Schindelin, I. Arganda-Carreras, E. Frise, V. Kaynig, M. Longair, T. Pietzsch, S. Preibisch, C. Rueden, S. Saalfeld, B. Schmid, J.-Y. Tinevez, D.J. White, V. Hartenstein, K. Eliceiri, P. Tomancak, A. Cardona, Fiji: an open-source platform for biological-image analysis, Nat. Methods 9 (2012) 676.

[16] P. Bilski, B. Marczewska, Y. Zhydachevskii, Radiophotoluminescence spectra of lithium fluoride TLDs after exposures to different radiation modalities, Radiat. Meas. 97 (2017) 14–19.

[17] L. Oster, S. Druzhyna, Y.S. Horowitz, Optically stimulated luminescence in LiF:Mg,Ti: Application to solid-state radiation dosimetry, Nucl. Instrum. Methods A 648 (2011) 261–265.

[18] J. Cardinale, Histogram-based background subtractor for ImageJ, ETH Zurich, 2010.

[19] S. Greilich, L. Grzanka, N. Bassler, C.E. Andersen, O. Jäkel, Amorphous track models: a numerical comparison study, Radiat. Meas. 45 (2010) 1406–1409.

[20] M. Niklas, M. Henrich, O. Jäkel, J. Engelhardt, A. Abdollahi, S. Greilich, STED microscopy visualizes energy deposition of single ions in a solid-state detector beyond diffraction limit, Phys. Med. Biol. 62 (2017) N180.